Cumhuriyet Sci. J., 46(1) (2025) 132-141
DOI: https://doi.org/10.17776/csj.1565431

Cumhuriyet Science Journal

| csj.cumhuriyet.edu.tr | Founded: 2002 ISSN: 2587-2680 e-ISSN: 2587-246X Publisher: Sivas Cumhuriyet University

Thermophysical Properties of Directionally Solidified the Zn-Mg-Al Eutectic Alloy and the Effect of Growth Rates on Electrical Properties

Ümit Bayram [1,2,a,*]

[1] *Central Research Facility (AGU-CRF), Abdullah Gül University, Kayseri, Türkiye*
[2] *Nanotechnology Application and Research Center (ERNAM), Erciyes University, Kayseri, Türkiye*
**Corresponding author*

Research Article

History
Received: 11/10/2024
Accepted: 03/01/2025

ABSTRACT

The study aimed to investigate the effect of growth rates (V) on the electrical properties of a Zn–3.0 Mg–2.5 Al (wt.%) eutectic alloy. The alloy was directionally solidified at four different growth rates ranging from 8.28 to 164.12 µm/s. Directional solidification experiments were conducted using a Bridgman-type solidification furnace, which was employed for controlled solidification and minimizing undesirable casting defects, following the alloy's production and casting process. The electrical resistivity (ρ) of the samples, measured using the Four-Point Probe Method (FPPM) available in the laboratory, exhibited an increasing trend ranging from 72.80 to 96.20 (nΩm) with rising growth rates. In other words, the electrical conductivity of the Zn–Mg–Al eutectic alloy varies inversely with the growth rate. Additionally, the thermophysical properties of the eutectic alloy in the casting phase were determined using differential scanning calorimetry (DSC): ΔHf (the fusion enthalpy), ΔCp (the specific heat) and TM (the melting point) (26.69 J/g, 0.043 J/gK, 618.92 K, respectively). The results obtained for the Zn–Mg–Al eutectic alloy reveal that, when compared to Zn-Al-based alloys produced under similar experimental conditions, the elements comprising the alloy and mass proportions lead to microstructural changes, which in turn affect its electrical conductivity.

Keywords: Zn–Mg–Al alloys, Directional solidification, Electrical resistivity, Thermophysical properties.

[a] *umit.bayram@agu.edu.tr* *https://orcid.org/0000-0001-8760-8024*

Introduction

Globally, renewable energy sources are being promoted as a measure to address the global challenges associated with heating and energy consumption. The use of wind and solar energy as primary power sources has seen significant growth in recent years, leading to an increased demand for systems that facilitate the adjustment of electricity generation, particularly from thermal power plants. Thermal energy storage systems are highlighted as a viable solution due to their advantages in energy efficiency and cost [1]. The capacity of energy storage in thermal systems is directly related to the selection of suitable thermal storage materials. Among thermal storage materials, eutectic alloys are preferred due to several superior properties: reduced phase separation compared to non-eutectic alloys, higher energy density due to intermetallic phase formation than pure metals, and superior thermal conductivity compared to inorganic salts [2,3].

Eutectic alloys also play a significant role in sustainable transportation by providing high strength and durability in the automotive industry while increasing fuel efficiency due to their lightweight properties. In other words, reducing vehicle weight is recognized as an effective method for improving fuel consumption in the automotive sector [4,5]. To achieve this, priority is given to materials such as aluminum alloys, which are lighter than steel. However, the primary challenge regarding efficiency and cost arises from applying these materials to the entire vehicle body. A key solution to this issue involves using multi-material structures incorporating zinc-aluminum (Zn-Al) based eutectic alloys with high strength and rigidity. In addition to their applications in automotive components, these alloys enable significant usage in various important applications, such as radio frequency circuits, disk drives, portable computers, phone antennas, and high-quality filters, due to their superior properties [6-8]. Furthermore, to obtain a coating material with excellent surface corrosion resistance and protective capabilities, zinc-based coatings with varying Al and Mg contents are widely used in the market [9-11].

The solidification microstructure is a critical foundational stage in the material preparation and shaping process, which typically directly determines the final performance and service life of the material. For this reason, eutectic alloys, which are frequently used by researchers and the casting industry, possess not only superior mechanical properties and casting capabilities but also low melting points [12-14]. In eutectic alloys, the solidification process begins when the temperature of the liquid reaches the eutectic temperature. At this stage, the liquid phase starts to transform into two or more solid phases. Directional solidification, on the other hand, is a model of the transition from liquid phase to solid phase and generally encompasses scenarios in which the temperature distribution is arranged in a specific linear manner. This process allows for the investigation of

different growth rates during solidification due to the temperature gradient within the alloy. Furthermore, directional solidification is employed to understand the factors affecting the temperature gradient and growth rates during the solidification process of eutectic alloys. In summary, while eutectic alloys form two or more solid phases during the transition from liquid phase to solid phase at a specific temperature, directional solidification serves as a model to help understand the effects of this solidification process on temperature and time. These two concepts are evaluated together to optimize metallurgical processes and achieve the desired microstructure.

The Bridgman-type controlled solidification technique is one of the fundamental methods used for the controlled directional solidification of metals and alloys. This technique plays a significant role in both fundamental research and industrial applications, particularly in the production of high-quality crystals and alloys. Undesirable casting defects in zinc and aluminum-based alloys can be minimized to the lowest levels using the Bridgman-type controlled solidification technique, as detailed in the literature [15,16].

According to the results obtained from studies on binary and multicomponent eutectic alloys in the literature [17-27], investigations related to directional solidification were predominantly conducted using Bridgman-type controlled solidification equipment within a standard growth rate range of 8-250 µm/s. Following the determination of solidification parameters (V, G, C_o) from the experimental results, the effects of growth rate on the microstructure, mechanical, thermal, and electrical properties were examined. In this context, the primary aim of the study is to experimentally perform directional solidification studies of the Zn–3.0 Mg–2.5 Al (wt.%) eutectic alloy within a fixed temperature gradient (G=4.58 K/mm) and a growth rate range of V=8.28–164.12 µm/s, and to elucidate the relationship between the growth rate values and the changes in electrical resistivity (ρ) using linear regression analysis. Additionally, another significant objective of this study is to determine the thermophysical properties of the eutectic alloy in the casting phase, such as the fusion enthalpy (ΔH_f), the specific heat difference between solid and liquid (ΔC_p), and the melting point (T_M), using a Simultaneous Thermal Analyzer (STA 8000). Finally, the results obtained for the Zn–Mg–Al eutectic alloy will be compared with Zn-Al-based alloys produced under similar experimental conditions, and the effects of changes in the microstructural arrangement on the electrical properties of the alloy will be discussed.

Materials and Methods

Alloy Preparation, Casting, and Solidification Experiments

The most critical part of the experimental procedures followed in this study includes the homogeneous preparation of the alloy, the execution of directional solidification experiments, and the measurement of solidification parameters (G-constant and V) thereafter, as well as the observation and characterization of the microstructure. Initially, high-purity materials were utilized to prevent impurities from accumulating at the interface and to avoid deterioration of the microstructure. These materials consisted of Alfa Aesar - 99.99% pure aluminum and 99.95% pure zinc, and Sigma-Aldrich - ≥99.9% pure magnesium. The appropriate amounts of Zn–3.0 Mg–2.5 Al (wt.%) eutectic alloy were weighed using a precision balance with a sensitivity of ±0.1 mg.

Before the casting of the alloy, a vacuum melting furnace was used to prevent metal oxidation and ensure the formation of a completely molten alloy. This furnace is equipped with a specially designed temperature controller that allows for a temperature accuracy of ±2 °C up to a maximum of 1100 °C, and the melting process is conducted under a pressure of 10^{-3} mbar with the help of a vacuum pump. Due to its superior properties, such as resistance to reaction with metallic materials, ease of processing through engineering applications, and a very high melting temperature (approximately 4000 °C), *Morgan-brand* graphite was preferred for the experimental equipment used before and after casting, including mixing rods, sample molds, and melting pots.

A specially designed casting furnace was utilized for the pouring of the obtained molten alloy and its unidirectional (linear) solidification within the sample molds. The prepared sample molds (Length: 200 mm, ID: 4.0 mm, OD: 6.35 mm) were placed inside the furnace, and the furnace temperature was raised to approximately 100-150 °C above the alloy's melting temperature (~345 °C) before casting. To ensure complete filling of the pots and to prevent one of the undesired casting defects known as shrinkage cavities, solidification was achieved using a graphite rod in 8–10-minute intervals. Simultaneously, while the lower heating zone within the casting furnace was cooled, the upper heating zone was maintained at a high temperature, allowing for unidirectional (linear) solidification within the sample molds. The alloy was allowed to cool for approximately one day, and the sample molds filled with the eutectic alloy were made ready for use in controlled solidification experiments.

At the beginning of the solidification experiments, the cast samples were placed in a Bridgman-type solidification furnace equipped with a protective graphite cylinder at the top. The block diagram of the experimental setup and its visual representation in the laboratory are shown in Figures 1(a) and 1(b). The directional solidification experiments of the samples were conducted using four different synchronous motors with withdrawal rates of 1 (V = 8.28 µm/s), 5 (V = 43.56 µm/s), 10 (V = 87.69 µm/s), and 20 rpm (V = 164.12 µm/s). Many technical details, from the production of alloy samples to the use of equipment shown in the block diagram in Fig. 1 and the calculations performed, as well as information regarding the Bridgman-type solidification furnace, have been provided in detail in previous studies [18, 28, 29].

The controlled solidification furnace was set to the desired temperature (~500 °C) using a temperature

controller, and the attainment of this temperature was monitored with a temperature recorder and thermocouples. A waiting period of approximately 2-3 hours was implemented to stabilize the temperature flow. The driver motor system was then activated to initiate the experiment, after which the solidified sample, approximately 10-12 cm in length, was quickly withdrawn into the cold zone containing the internal water reservoir, where it underwent an abrupt cooling process known as quenching. To ensure the effectiveness of the rapid cooling, the withdrawal process was conducted very quickly, and the temperature of the internal reservoir, designed to create a temperature gradient, was meticulously controlled. These experimental procedures were conducted at four different growth rates, with two samples for each rate. The reason for performing two samples is to determine the growth rates and the temperature gradient of the material by placing thermocouples inside alumina tubes. Samples containing alumina tubes would not yield reliable results for the electrical properties to be measured. Therefore, two experiments were conducted for each growth rate under the same conditions.

.

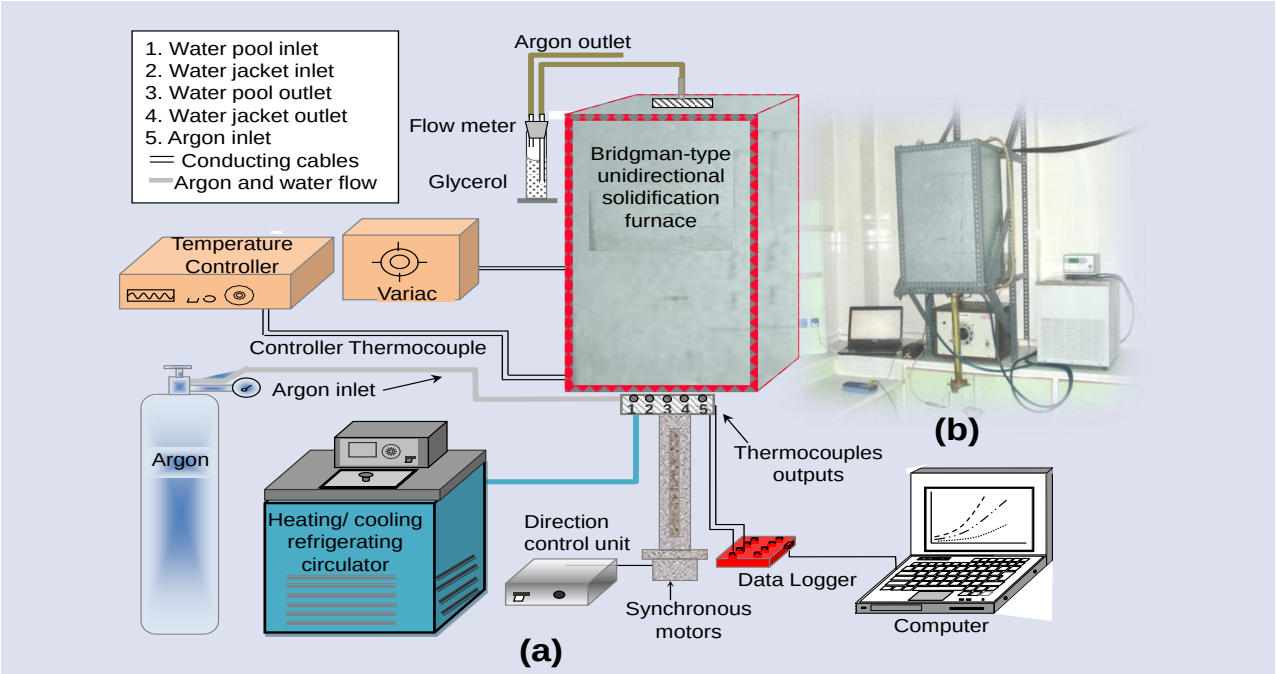

Figure 1. (a) Block diagram of the experimental setup, and (b) photograph inside the laboratory.

The solidified alloys were carefully removed from the graphite crucibles without causing any damage. To identify the microstructure and phases of all samples, the *Struers-Minitom* cutting tool and a *Struers* diamond cutter (127 mm diameter, 0.4 mm thickness) were used to cut the samples to the desired sizes. An important consideration in this process is the necessity of employing a cutting technique that causes minimal structural change and generates the least amount of heat. The samples were polished using sandpapers that gradually changed from coarse to fine, containing silicon carbide (SiC) grains and magnetite powder (320, 500, 1000, 2000 grit). During the polishing process, carried out with an automatic polishing robot (*Struers TegraPol-15*), care was taken to ensure that the surface of each sample remained flat and that deep scratches were removed after each polishing stage. The sections prepared for metallographic procedures were molded using epoxy and hardener chemicals at a 7:1 ratio. Although the surface of the sample appeared smooth, shiny, and mirror-like after polishing, it is not possible to conduct examinations without creating contrast on the sample surface. For microstructure analysis, the samples required etching. Finally, the Zn–3.0 Mg–2.5 Al (wt.%) eutectic alloy was etched by immersion in a Keller etchant (1.5 ml Hydrochloric acid (HCl), 1 ml Hydrofluoric acid (HF), 2.5 ml Nitric acid (HNO_3), 95 ml water (H_2O)) for 40-45 seconds, preparing it for microstructure analysis.

Microstructure, Phase Analysis, and Solidification Parameters (G and V)

Following metallographic processes such as cutting, polishing, molding, ultrasonic cleaning, and etching of the samples, characterization studies were conducted. To identify the resulting microstructures and phases, images and data obtained from SEM (Scanning Electron Microscope - Zeiss GeminiSEM 300) and SEM-EDX (Energy Dispersive X-ray Spectroscopy) were utilized. Before the microstructure analysis using SEM, the surface of the samples, which were embedded in epoxy, was placed in a Quorum-Q150R Plus coating device and coated with a gold (Au) layer approximately 10-20 nm thick under vacuum to ensure more efficient scattering of the electron beam from the surface, thereby improving image resolution. The gold-coated samples were then positioned on the sample stage within the SEM, and photographs were taken from suitable areas where the phases

exhibited high contrast and could be easily distinguished. EDX-point analysis was performed on the phases to determine the composition of each phase.

To measure the temperature of the alloy, three K-type thermocouples (diameter: 0.25 mm) insulated with capillary ceramic alumina tubes were fixed at intervals of 10 mm. Using the data recorded by a computer-connected data logger for ΔT, ΔX, and Δt, the temperature gradient (G = ΔT/ΔX) and growth rate (V = ΔX/Δt) values were calculated. Here, ΔT (°C) is defined as the difference in temperature values measured by any two thermocouples, ΔX (mm) is the predetermined distance between the thermocouples, and Δt (s) is defined as the transition time of the solid-liquid interface across any two thermocouples. Since the distance between the cold and hot regions of the furnace was kept constant and the experimental parameters were not altered during the solidification process, the temperature gradient value (G) at the solid-liquid interface could be maintained constant. In addition to obtaining the values of Δt, ΔX, and ΔT, detailed information regarding the calculations of V and G has been provided in previous studies [18, 28, 29].

Electrical Resistivity (ρ) Measurement and Details

Electrical resistivity and conductivity are characteristic properties of materials that need to be known. Electrical conductivity can be determined using the relationship between the voltage and current measured across the sample, the calculated resistivity value, and the geometric structure of the sample. Additionally, when determining the electrical resistivity of a homogeneous sample, it is essential to know the geometric properties of the material as well. The expression for electrical resistivity can be given as follows [30]:

$$\rho = \frac{V}{I} G \quad (1)$$

G is defined here as a correction factor dependent on the geometric structure (Resistivity Correction Factor, RCF). This coefficient varies based on factors such as the magnitude of the surface area, the structure of the sample's edge boundaries, the thickness of the sample, its geometric configuration, and the arrangement and position of the contacts on the sample [31]. The electrical resistivity values of each sample (20 mm in length and 4 mm in diameter) were measured using the four-point probe method (FPPM), as shown in the photograph and block diagram of the measurement system presented in Fig. 2, depending on the growth rate of the eutectic alloy.

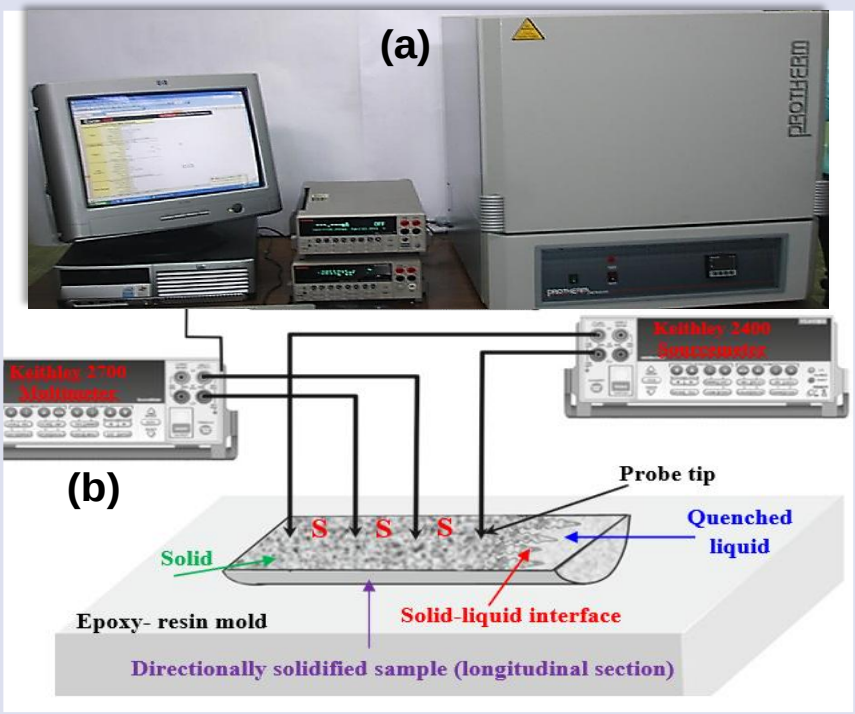

Figure 2. Four-point probe method (FPPM), (a) Photograph of the measurement system, (b) Schematic diagram.

In this study, the four-point probe method (FPPM) was equipped with a Keithley 2700 multimeter and a Keithley 2400 programmable power supply. The method is based on measuring the voltage value against the current applied to the sample through four platinum wires with a diameter of 0.5 mm, positioned within a Protherm-brand ash furnace. The platinum wires were directly in contact with the surface of the bar-shaped samples at four electrical contact points. Two of the probes were used to measure the potential difference between two points, while the other two were used for sourcing the current. FPPM was preferred in this study due to its superior characteristics, such as eliminating measurement errors arising from the spreading resistance under each probe,

probe resistance, and contact resistance between each platinum probe and the material [32]. In summary, the resistances of the contacts used do not affect the measurement, and the calculated value represents only the resistivity of the sample. To enhance the reliability of the results in determining the electrical resistivity value, a minimum of 40-50 measurements were taken across the same sample to obtain an average value. Details regarding the measurement and use on the sample surface are provided in the work conducted by Smiths [32].

Thermophysical Properties (ΔH_f, ΔC_p and T_M)

The thermophysical properties of the Zn–3.0 Mg–2.5 Al (wt.%) eutectic alloy were determined in the casting phase (before solidification) using a Simultaneous Thermal Analyzer (STA 8000). This method encompasses techniques in which a physical property of the analyzed sample is measured as a function of temperature, or the heat released or absorbed in a chemical reaction is monitored. Specifically, properties such as phase transition, melting, glass transition, and crystallization are measured directly, while ΔC_p (the specific heat difference between solid and liquid, or the specific melting heat—the energy required for the melting of unit mass), ΔH_f (the fusion enthalpy), and T_M (the melting temperature) are calculated from the obtained curves. A suitable amount (8.81 mg) of the Zn–Mg–Al eutectic alloy was placed into the device and heated up to 700 K at a rate of 10 K/min under a nitrogen atmosphere. The ΔH_f value was calculated using the area under the peak derived from the alloy data:

$$\Delta H = \frac{Area}{m} \quad (2)$$

The definition of enthalpy from the equation indicates that it is the energy required for the melting of unit mass (m). The ΔC_p value is calculated using the equation:

$$\Delta C_p = \frac{\Delta H_f}{T_M} \quad (3)$$

Results and Discussion

SEM Analysis and Phase Characterization

In this study, the composition of the Zn–Mg–Al alloy to be investigated at the eutectic point was determined based on the work conducted by Kim *et al.* [33] using CALPHAD analysis. Accordingly, the composition of the alloy was selected as Zn–3.0 Mg–2.5 Al (wt.%), and the phases involved in the eutectic reaction at this point are as follows: E (eutectic reaction): L↔(μ-Zn) + $MgZn_2$ + (α-Al). For the determined eutectic Zn–Mg–Al alloy, microstructure (SEM) images obtained from the cross-sections of directionally solidified samples at four different growth rates are presented in Fig. 3. These images, taken at equal magnification values, demonstrate that the distance between the phases forming the alloy decreases with increasing growth rates, leading to a transition towards a more irregular structure.

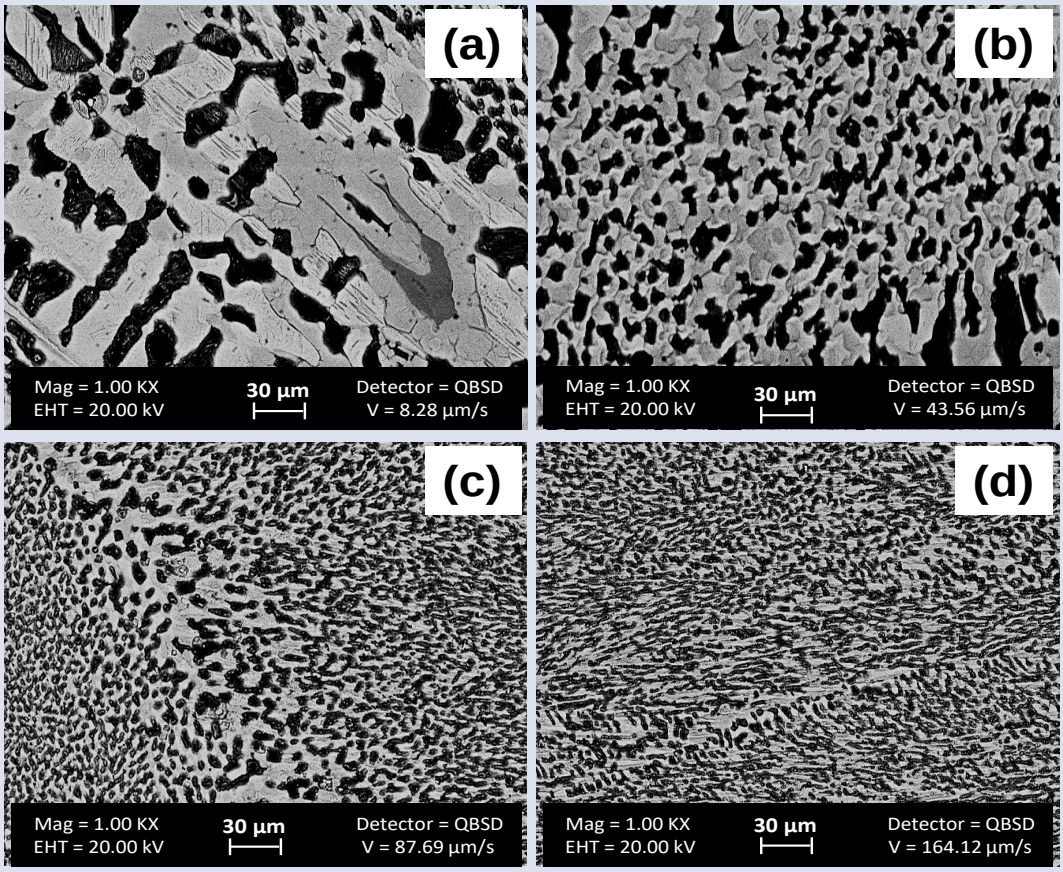

Figure 3. SEM images of cross sections for directionally solidified Zn–3.0 Mg–2.5 Al (wt.%) eutectic alloy. (a) V= 8.28 µm/s, (b) V= 43.56 µm/s, (c) V= 87.69 µm/s, (d) V= 164.12 µm/s.

As a result of solidification experiments, certain phases have separated in the phase diagram [33] as defined and point composition analyses of each distinct phase of the studied eutectic alloy have been conducted. The analyses revealed that three different phases—grey, black, and white—grew eutectically in the Zn–Mg–Al eutectic alloy, as observed from the microstructural photographs presented in Fig. 3. The quantitative chemical composition analyses obtained from SEM-EDX results are shown in Fig. 4.

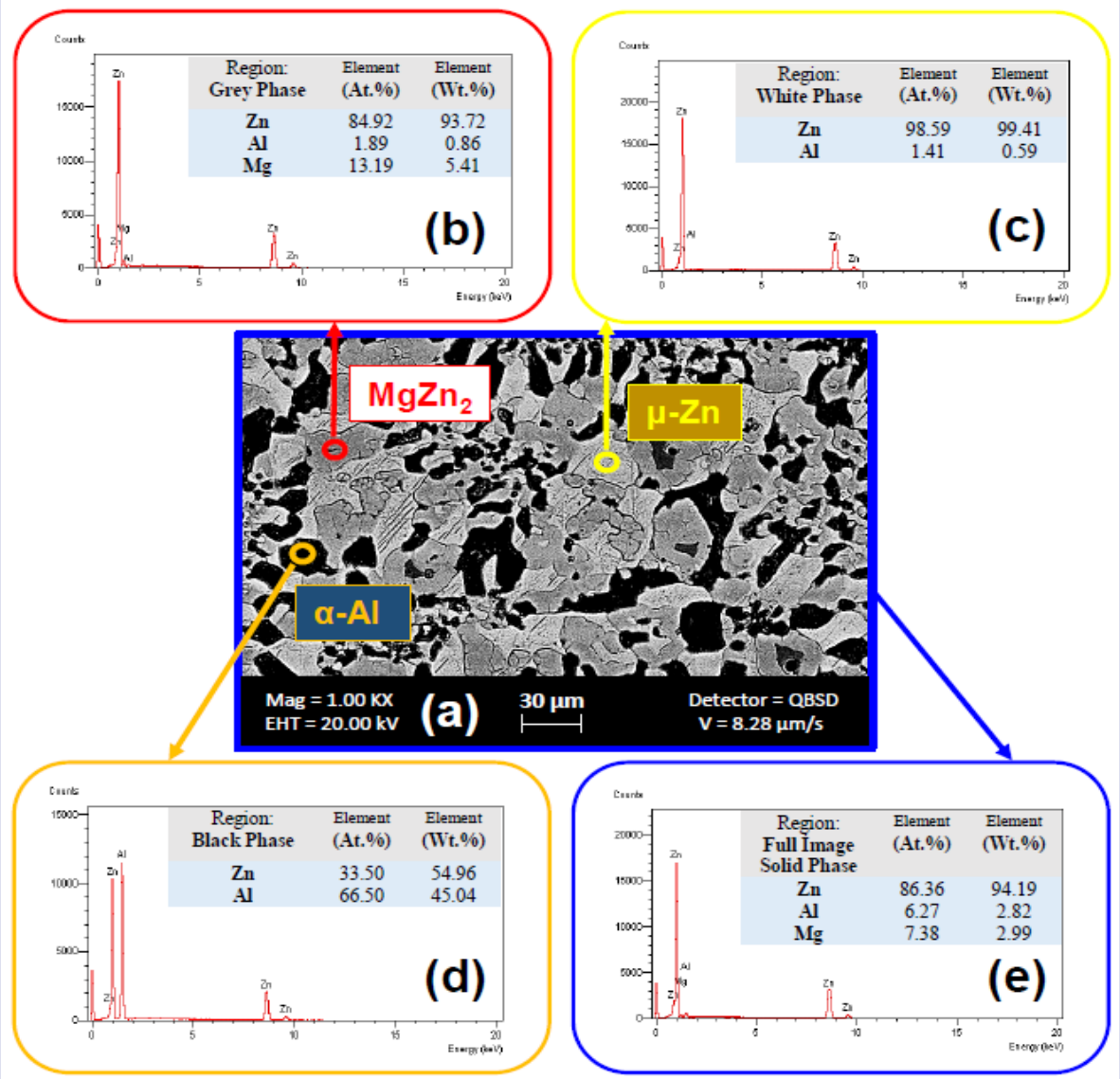

Figure 4. (a) Transverse SEM image of the eutectic alloy obtained at a growth rate of 8.28 μm/s. SEM-EDX results for the phases in the Zn–3.0 Mg–2.5 Al (wt.%) eutectic alloy: (b) Grey phase; $MgZn_2$ intermetallic phase, (c) White phase; η-Zn primary (matrix) phase, (d) Black phase; α-Al solid solution phase, and (e) EDX result obtained from the solid phase in the full image.

Upon examining the results in Fig. 4, it can be observed that the grey phase (Fig. 4b) corresponds to the MgZn2 intermetallic phase (Zn–5.41 Mg–0.86 Al (wt.%)), the white phase (Fig. 4c) corresponds to the η-Zn primary (matrix) phase (Zn–0.59 Al (wt.%)), and the black phase (Fig. 4d) corresponds to the α-Al solid solution phase (Zn–45.04 Al (wt.%)). The EDX result obtained from the solid phase in Fig. 4e is Zn–2.99 Mg–2.82 Al (wt.%), which is found to be quite close and consistent with the eutectic composition prepared in this study (Zn–3.0 Mg–2.5 Al (wt.%)). This consistency suggests that the alloy was produced homogeneously.

The Variation of Electrical Resistivity Values with Growth Rates

The other significant aim of this study is to investigate the electrical properties of the Zn–Mg–Al eutectic alloy, which is frequently used in both industrial and technological applications, and to reveal the effects of growth rates. To this end, each sample was placed in an ash furnace at room temperature, ensuring complete contact of four platinum wires with the sample. The electrical resistivity (ρ) values were then measured in nΩm. To enhance statistical reliability, at least 40-50 measurements were taken for each sample, and the averages were included in the calculations. Subsequently,

the relationship between the measured electrical resistivity values and the varying growth rates was established using linear regression analysis

In this study, the variation of electrical resistivity values with growth rate on a logarithmic scale is linear within the range of growth rates used (V = 8.28–164.12 µm/s), and the proportional equation can be obtained through linear regression analysis as follows:

$$\rho = K_1 . V^{-n} \ \ (for\ constant\ G) \qquad (4)$$

where K_1 is the proportionality constant and n is the exponent of the growth rate. The relationship between the electrical resistivity values obtained from the cross-section and all growth rates (V = 8.28–164.12 µm/s) was determined for the directionally solidified Zn–3.0 Mg–2.5 Al (wt.%) eutectic alloy using the following equation (Fig. 5):

$$\rho = 58.70\ V^{0.09} (n\Omega m) \qquad (5)$$

From the SEM images provided in Fig. 3, it can be observed that increases in the growth rate significantly alter the eutectic microstructure, thereby affecting the other properties of the alloy. In this study, it was concluded that the electrical resistivity values measured using FPPM also increase with the rise in growth rates under a constant temperature gradient (G = 4.58 K/mm). In other words, the electrical conductivity (σ = 1/ρ) of the Zn–3.0 Mg–2.5 Al (wt.%) eutectic alloy varies inversely with the growth rates. The highest electrical resistivity value (96.20 nΩm) was obtained at the highest growth rate (164.12 µm/s), while the lowest electrical resistivity value (72.80 nΩm) was measured at the lowest growth rate (8.28 µm/s).

To compare and discuss the results obtained in this study, the electrical resistivity values and proportional equations of directional solidified Zn–Al-based eutectic alloys under similar experimental conditions are shown in Fig. 5 [21, 23, 25]. The exponent value of 0.09 and the proportionality constant of 58.70 obtained from the electrical resistivity measurements for the growth rates are consistent with the values obtained for the Zn–5.0 Al–0.8 Sb (wt.%) eutectic alloy [23]. However, these values differ significantly from the exponent values of the eutectic alloys containing Bi [21] and Cu [25] (0.11 and 0.06, respectively). The reason for the exponent value being higher for the Zn–5.0 Al–0.5 Cu (wt.%) [25] alloy and lower for the Zn–5.0 Al–0.2 Bi (wt.%) [21] alloy can be attributed to the solubility of the copper and bismuth elements within the zinc matrix rather than the mass proportions of the alloying elements, which prevents the formation of any intermetallic phases. The results of this study and the article conducted for the Zn–5.0 Al–0.8 Sb (wt.%) [23] eutectic alloy, clearly show the formation of $MgZn_2$ and AlSb intermetallic phases in the microstructure images.

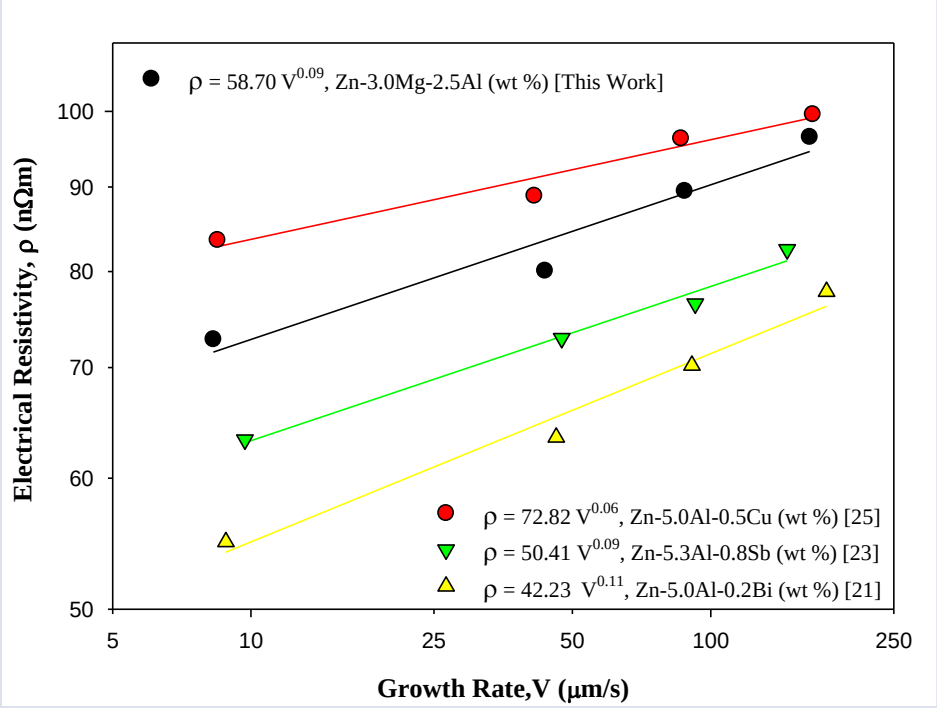

Figure 5. The variation of electrical resistivity values as a function of growth rates for directionally solidified Zn–Mg–Al eutectic alloy under a constant temperature gradient and compared with the experimental results of previous Zn-Al based alloys.

The effect of intermetallic phases on the electrical properties of alloys is influenced by factors such as microstructure, phase distribution, and atomic structure [34,35]. Consequently, the presence and characteristics of intermetallic phases play a critical role in determining the electrical performance of alloys. Firstly, intermetallic phases generally reduce the electrical conductivity of the alloy. This reduction is due to the distinct atomic

structures and bonding of these phases. The voids and irregularities within these structures lead to a decrease in electron mobility [36]. On the other hand, changes in the alloy's microstructure resulting from intermetallic phases, along with grain boundary and interphase interactions, also impact electrical conductivity. An increase in the grain boundary area can hinder electron flow, thereby reducing conductivity [37]. Both studies referenced, involving these intermetallic phases (MgZn2 [this study] and AlSb [23]), may contribute to the alloys exhibiting similar electrical properties.

The Evaluation of Thermophysical Properties

Understanding the thermal properties of alloys, such as melting point (TM), the specific heat difference between solid and liquid (ΔCp), the fusion enthalpy (ΔHf) and crystallization temperature, is crucial for determining their suitability for various applications. The DSC (Differential Scanning Calorimetry) graph obtained using the Simultaneous Thermal Analyzer (STA 8000) measures energy changes during the heating processes of the alloy, helping to identify phase transitions (such as melting and crystallization) and related characteristics. For the temperature program of the device, a heating rate of 10 K/min was set, with a starting temperature of 400 K and an ending temperature of 700 K. Thus, within this specified temperature range, the heat flow curve (DSC graph) of the eutectic alloy consisting of 8.18 mg Zn–3.0 Mg–2.5 Al (wt.%) was obtained under a constant nitrogen atmosphere (Fig. 6).

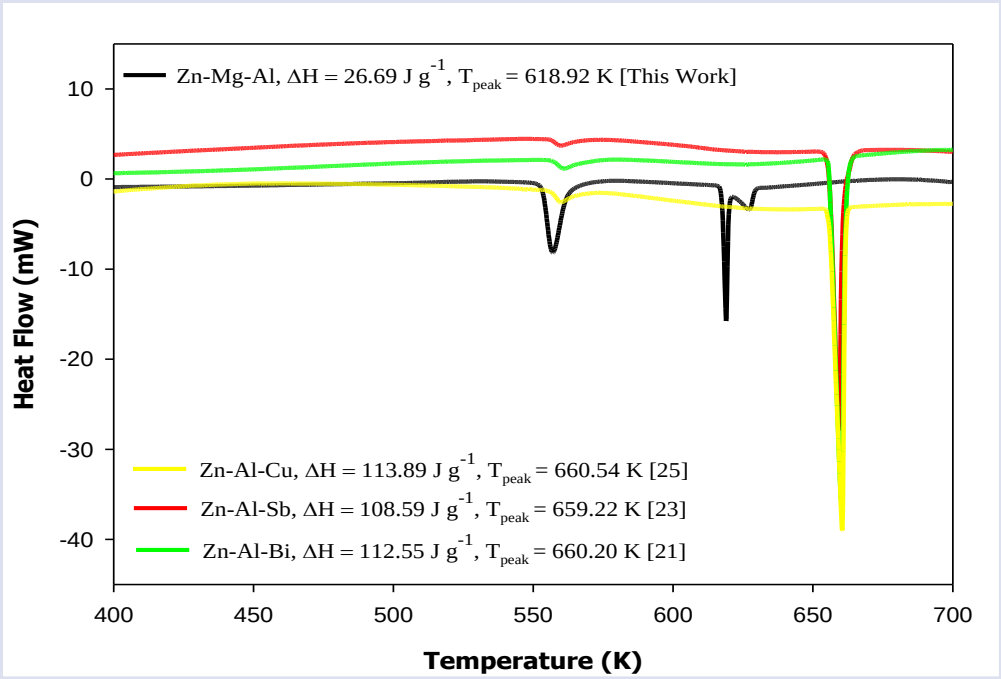

Figure 6. The variation of electrical resistivity values as a function of growth rates for directionally solidified Zn–Mg–Al eutectic alloy under a constant temperature gradient and compared with the experimental results of previous Zn-Al based alloys.

The melting temperature (T_{peak}) of the Zn–3.0 Mg–2.5 Al (wt.%) eutectic alloy was determined to be 618.92 K. The values of ΔH_f and ΔC_P were found to be 26.69 $J \cdot g^{-1}$ and 0.043 $J \cdot g^{-1} \cdot K^{-1}$, respectively. The calculated value of 26.69 $J \cdot g^{-1}$ is approximately four times lower than the values reported for Zn-Al-Cu [25], Zn-Al-Sb [23], and Zn-Al-Bi [21] alloys, which are 113.89 $J \cdot g^{-1}$, 108.59 $J \cdot g^{-1}$, and 112.55 $J \cdot g^{-1}$, respectively. This difference can be attributed to the presence of magnesium (~8.9 $k \cdot J \cdot mol^{-1}$) in the Zn–3.0 Mg–2.5 Al (wt.%) eutectic alloy, which has a lower fusion enthalpy compared to copper (~13.1 $k \cdot J \cdot mol^{-1}$), antimony (~19.7 $k \cdot J \cdot mol^{-1}$), and bismuth (~10.9 $k \cdot J \cdot mol^{-1}$). Thus, the inclusion of magnesium in the alloy reduces the overall fusion enthalpy, resulting in a lower melting point and facilitating the melting process [38]. A further difference is observed in the ΔC_P values. Due to its low density, magnesium contributes to a reduction in the overall density of the alloy, which can lead to a decrease in ΔC_P [39, 40].

Conclusion

Due to its superior properties such as high strength, lightweight, and corrosion resistance, the Zn–3.0 Mg–2.5 Al (wt.%) eutectic alloy is used in various industrial applications. Solidification studies were conducted using a Bridgman-type solidification furnace with a constant temperature gradient (G = 4.58 K/mm) and a growth rate range of V = 8.28–164.12 µm/s, at a furnace temperature of approximately 500 °C. Scanning Electron Microscopy (SEM) images were obtained to elucidate the microstructure and characterize the phases constituting the alloy, with quantitative chemical composition analyses (SEM-EDX) presented in graphical form for each phase. The electrical resistivity values of the solidified samples, dependent on each growth rate, were measured using FPPM, and the relationship between the growth rates and electrical resistivity values was established through linear regression analysis. The significant results emerging from this study can be summarized as follows:

1. It has been concluded that as the growth rates increase, the electrical resistivity values also rise proportionally. The highest electrical resistivity value (96.20 nΩm) was measured at the highest growth rate (164.12 µm/s), while the lowest electrical resistivity value (72.80 nΩm) was observed at the lowest growth rate (8.28 µm/s). In other words, the electrical conductivity (σ = 1/ρ) of the Zn–3.0% Mg–2.5% Al (wt.%) eutectic alloy exhibits an inverse relationship with the growth rates. Furthermore, the equation obtained from linear regression analysis ($\rho = 58.70\ V^{0.09}(n\Omega m)$) indicates that both the exponential value and the proportionality constant may reflect differences observed in some studies in the literature, which could be attributed to the $MgZn_2$ intermetallic phase. The differences arising from the $MgZn_2$ intermetallic phase can be attributed to two characteristics: (1) the distinct atomic structure and bonding of the $MgZn_2$ intermetallic phase, and (2) the emergence of more and tighter phase boundaries due to the increase of grain boundaries, which can hinder the passage of electrons and thus decrease conductivity.
2. The thermophysical properties of the Zn–3.0 Mg–2.5 Al (wt.%) eutectic alloy were determined from the DSC graph obtained using the PerkinElmer-STA8000 model device (T_M = 618.92 K, ΔH_f = 26.69 $J \cdot g^{-1}$, ΔC_P = 0.043 $J \cdot g^{-1} \cdot K^{-1}$), and the results were compared with Zn-Al based studies in the literature. It was noted that the presence of magnesium in the Zn–3.0 Mg–2.5 Al (wt.%) alloy reduced the overall fusion enthalpy compared to other Zn-Al based alloys, resulting in a lower melting point. Additionally, by making a similar comparison with the ΔC_P value, it was emphasized that magnesium, being a low-density metal, decreases the overall density of the alloy, which could lead to a reduction in ΔC_P.

Conflict of interest

The author declares no conflict of interest in this work.

Acknowledgment

The researcher is grateful to Professor Necmettin Maraşlı and his team for their support in conducting the experimental parts of the study in the Solid-State Physics-I laboratory.

References

[1] Yamamoto K., Domoto K., Tobo M., Kawamizu T., Yamana T., Ota Y., Thermal Storage System to Provide Highly Efficient Electric Power Resilience in The Era of Renewable Energy, *Mitsubishi Heavy Industries Tech. Rev.,* 57 (1) (2020) 1–11.

[2] Nazir H., Batool M., Bolivar Osorio F. J., Isaza-Ruiz M., Xu X., Vignarooban K., Phelan P., Inamuddin, Arunachala I., Kannan A. M., Recent Developments in Phase Change Materials for Energy Storage Applications: A Review, *Int. J. Heat Mass Trans.*, 129 (2019) 491–523.

[3] Zhou, C., Wu S., Medium-and High-Temperature Latent Heat Thermal Energy Storage: Material Database, System Review, and Corrosivity Assessment. *Int. J. Energy Research,* 43 (2019) 621–661.

[4] Hirose A., Trends of Applications and Joining Technologies of Aluminum Alloys in Automobiles, *Journal of JSAE*, 61 (2007) 18-23.

[5] Sasabe S., Dissimilar Metal Joining Technology of Aluminum Alloy to Steel, *Journal of JSAE*, 61 (2007) 24-29.

[6] Porter D.A., Easterlirng K.E., Phase Transformations in Metals and Alloys, 2nd Ed., CRC Press, London, (1992).

[7] Caram R., Milenkovic S., Microstructure of Ni–Ni3Si eutectic alloy produced by directional solidification, *J. Crys. Growth*, 198–199 (1) (1999) 844-849.

[8] Fu H.Z., Liu L., Progress of Directional Solidification in Processing of Advanced Materials, *Mat. Sci. Forum*, 475–479 (2005) Zurich-Uetikon, Switzerland.

[9] Li Z., Li Y., Jiang S., Zhang J., Liu X., Zhang Q., Liu Q., Calculation and Experimental Verification of Zn–Al–Mg Phase Diagram. *Coatings*, 14 (4) (2024) 468.

[10] Delneuville P., Tribological Behaviour of ZnAl Alloys (ZA27) Compared with Bronze When Used as A Bearing Material with High Load and at Very Low Speed, *Wear*, 105 (4) (1985) 283-292.

[11] Auras R., Schvezov C., Wear Behavior, Microstructure, and Dimensional Stability of As-Cast Zinc-Aluminum/SIC (Metal Matrix Composites) Alloys, *Metall. Mat. Trans. A*, 35 (2004) 1579–1590.

[12] Kurz W., Fisher D.J., Fundamentals of Solidification, Chapter 5, 4th revised edition, Trans. Tech. Publications Ltd., Bäch, Switzerland, (1998).

[13] Zhang Y., Song C., Zhu L., Zheng H., Zhong H., Han Q., Zhai Q., Influence of Electric-Current Pulse Treatment on the Formation of Regular Eutectic Morphology in an Al-Si Eutectic Alloy, *Metall. Mat. Trans. B*, 42 (2011) 604–611.

[14] Kakitani R., de Gouveia G.L., Garcia A., Cheung N., Spinelli J.E., Thermal Analysis During Solidification of an Al–Cu Eutectic Alloy: Interrelation of Thermal Parameters, Microstructure and Hardness, *J. Thermal Analy. Cal.,* 137 (2019) 983–996.

[15] Duffar T., Sylla L., Crystal Growth Processes Based on Capillarity. Chapter 6—Vertical Bridgman Technique and Dewetting, Wiley, New York, (2010) 355–411.

[16] Venkataraman R., Handbook of Radioactivity Analysis (4th edition). Chapter 4—Semiconductor detectors, Elsevier Inc., (2020) 458-459.

[17] Rios C.T., Oliveira M.F., Caram R., Botta F.W.J., Bolfarini C., Kiminami C.S., Directional and Rapid Solidification of Al–Nb–Ni Ternary Eutectic Alloy, *Mat. Sci. Eng. A,* 375–377 (2004) 565-570.

[18] Çadırlı E., Kaya H., Gündüz M., Directional Solidification and Characterization of the Cd–Sn Eutectic Alloy, *J. Alloys Comp.*, 431 (1-2) (2007) 171-179.

[19] Li X., Ren Z., Fautrelle Y., Zhang Y., Esling C., Morphological Instabilities and Alignment of Lamellar Eutectics During Directional Solidification Under a Strong Magnetic Field, *Acta Mat.*, 58 (4) (2010) 1403-1417.

[20] Cui C., Zhang J., Xue T., Liu L., Fu H., Effect of Solidification Rate on Microstructure and Solid/Liquid Interface Morphology of Ni–11.5 wt% Si Eutectic Alloy, *J. Mat. Sci. Tech.*, 31 (3) (2015) 280-284.

[21] Karamazı Y., Bayram Ü., Ata P., Aksöz S., Keşlioğlu K., Maraşlı N., Dependence of microstructural, mechanical and electrical properties on growth rates in directional solidified Zn-Al-Bi eutectic alloy, *Trans. Nonfer. Metals Soc. China*, 26 (9) (2016) 2320-2335.

[22] Zuo X., Zhao C., Zhang L., Wang E., Influence of Growth Rate and Magnetic Field on Microstructure and Properties of Directionally Solidified Ag-Cu Eutectic Alloy, *Materials*, 9 (7) (2016) 569.

[23] Bayram Ü., Karamazı Y., Ata P., Aksöz S., Keşlioğlu K., Maraşlı N., Dependence Of Microstructure, Microhardness, Tensile Strength and Electrical Resistivity on Growth Rates for Directionally Solidified Zn-Al-Sb Eutectic Alloy, *Int. J. Mat. Res.*, 107 (11) (2016) 1005-1015.

[24] Hötzer J., Steinmetz P., Dennstedt A., Genau A., Kellner M., Sargin I., Nestler B., Influence of Growth Velocity Variations on the Pattern Formation During the Directional Solidification of Ternary Eutectic Al-Ag-Cu, *Acta Mat.*, 136 (2017) 335-346.

[25] Maraşlı N., Bayram, Ü., Aksöz, S., The variations of electrical resistivity and thermal conductivity with growth rate for the Zn–Al–Cu eutectic alloy. *J. Mater. Sci.: Mater. Electron*, 32 (2021) 18212–18223.

[26] Yan J., Liu T., Wang M., Sun J., Dong S., Zhao L., Wang Q., Constitutional Supercooling and Corresponding Microstructure Transition Triggered by High Magnetic Field Gradient During Directional Solidification of Al-Fe Eutectic Alloy, *Mat. Charact.*, 188 (2022) 111920.

[27] Bayram Ü., Investigation of Changes in Microstructure and Microhardness Properties of Zn-Al Eutectic Alloy as a Result of Directionally Solidification at High Velocities, *Erciyes Uni. J. Ins. Sci. Tech.*, 40 (2) (2024) 408-419.

[28] Çadırlı E., Gündüz M., The Dependence of Lamellar Spacing on Growth Rate and Temperature Gradient in the Lead-Tin Eutectic Alloy, *J. Mat. Proc. Tech.*, 97 (2000) 74−81.

[29] Böyük U., Maraşlı N., Kaya H., Çadırlı E., Keşlioğlu K., Directional solidification of Al−Cu−Ag alloy, *App. Physics A*, 95 (2009) 923−932.

[30] Yamashita M., Resistivity Correction Factor for the Four-Probe Method, *J. Phys. E: Sci. Instrum.*, 20 (1987) 1454-1456.

[31] Caignan A.G., Holt E.M., New 1,4-dihydropyridine Derivates with Hetero, Saturated B Rings, *J. Chem. Cryst.*, 32 (2002) 315-323.

[32] Smits F. M., Measurement of Sheet Resistivities with the Four-Point Probe, *The Bell System Tech. J.*, 37 (1958) 711-718.

[33] Kim J. N., Lee C. S., Jin Y. S., Structure and Stoichiometry of Mg_xZn_y in Hot-Dipped Zn–Mg–Al Coating Layer on Interstitial-Free Steel, *Met. Mater. Int.*, 24 (2018) 1090–1098.

[34] Gancarz T., Pstrus J., Characteristics of Sn–Zn Cast Alloys with the Addition of Ag and Cu, *Arch. Metall. Mater.*, 60 (2015) 1603–1607.

[35] Kamal M., Meikhail M. S., El-Bediwi A. B., Gouda E. S., Study of Structural Changes and Properties for Sn–Zn9 Lead-Free Solder Alloy with Addition of Different Alloying Elements, *Rad. Eff. Defect Solids*, 160 (2005) 45–52.

[36] Lee W. B., Bang K. S., Jung S. B., Effects of Intermetallic Compound on the Electrical and Mechanical Properties of Friction Welded Cu/Al Bimetallic Joints During Annealing, *J. Alloys Comp.*, 390 (1-2) (2005) 212-219.

[37] Zhang L., Luo J., Zhang S., Yan J., Huang X., Wang L., Gao J., Interface Sintering Engineered Superhydrophobic and Durable Nanofiber Composite for High-Performance Electromagnetic Interference Shielding, *J. Mat. Sci. Tech.*, 98 (2022) 62-71.

[38] Abdullaev R. N., Agazhanov A. S., Khairulin A. R., Samoshkin D. A., Stankus S. V., Thermophysical Properties of Magnesium in Solid and Liquid States, *J. Eng. Thermo.*, 31 (2022) 384–401.

[39] Li S., Yang X., Hou J., Du W., A Review on Thermal Conductivity of Magnesium and its Alloys, *J. Magnes. Alloys*, 8 (2020) 78–90.

[40] Song J., She J., Chen D., Pan F., Latest Research Advances on Magnesium and Magnesium Alloys Worldwide, *J. Magnes. Alloys*, 8 (2020) 1–41.